PCCP

PAPER

View Article Online
View Journal | View Issue

Cite this: *Phys. Chem. Chem. Phys.*, 2015, **17**, 26346

Ultrafast charge separation and charge stabilization in axially linked 'tetrathiafulvalene–aluminum(III) porphyrin–gold(III) porphyrin' reaction center mimics†

Prashanth K. Poddutoori,*[a] Gary N. Lim,[b] Serguei Vassiliev[c] and Francis D'Souza*[b]

Received 13th August 2015,
Accepted 8th September 2015

DOI: 10.1039/c5cp04818d

www.rsc.org/pccp

The axial bonding ability of aluminum(III) porphyrin (AlPor) has been exploited to synthesize the vertically linked dyad 'aluminum(III) porphyrin–gold(III) porphyrin' (AlPor-Ph–AuPor$^+$) and the two corresponding self-assembled triads 'tetrathiafulvalene–aluminum(III) porphyrin–gold(III) porphyrin' (TTF-py→AlPor-Ph–AuPor$^+$ and TTF-Ph-py→AlPor-Ph–AuPor$^+$). The unique topology of these triads provides an excellent opportunity to investigate the sequential electron transfer in the perpendicular direction to the AlPor plane where the AlPor acts as a photosensitizer and primary electron donor while the AuPor and TTF serve as an electron acceptor and donor, respectively. The ground state properties of the dyad and triad suggest that there are no direct intramolecular interactions between the oppositely disposed AuPor and TTF units of the triad. However, the NMR and UV-visible absorption studies of the dyad reveal intermolecular interactions in non-coordinating solvents due to the coordination of counterion PF_6^- to the Al center of AlPor. Steady-state and femtosecond transient absorption studies of the dyad show that the lowest excited singlet state of AlPor (^{1}AlPor*) is strongly quenched by ultrafast electron transfer to AuPor$^+$ with a time constant of 3.16 ps. The resulting charge separated state (AlPor$^{+\bullet}$–AuPor$^\bullet$) decays to ground state biexponentially with time constants of 27.26 and 2557 ps. Analogously, upon photo-excitation the triads also produce the same primary radical pair (AlPor$^{+\bullet}$–AuPor$^\bullet$). However, the formed radical pair is further involved in a rapid hole transfer from AlPor$^{+\bullet}$ to TTF to form a stable final radical pair TTF$^{+\bullet}$–AlPor–AuPor$^\bullet$. The lifetime of the charge separated state exhibits an increase from 27.26 ps in AlPor-Ph–AuPor to 1393 ps in TTF-py→AlPor-Ph–AuPor$^+$ and 1484 ps in TTF-Ph-py→AlPor-Ph–AuPor$^+$. These results reveal successful charge stabilization in the self-assembled supramolecular reaction center mimics constructed *via* the axial linkage strategy.

1. Introduction

Photosynthesis is nature's most well-designed process, in which sunlight is converted into chemical energy.[1,2] In this process, the fundamental reactions such as photoinduced energy transfer (EnT) and electron transfer (ET) between photosynthetic molecular components are well optimized to drive the desired reactions towards conversion of solar energy into chemical energy. Over the last few decades, a significant amount of progress has been achieved in terms of understanding the factors that govern EnT and ET in photosynthesis by using multi-component synthetic models with the objective of tapping the solar energy for future energy needs.[3–17] Within these synthetic models, porphyrin (Por) molecules have emerged as promising building blocks for construction of multi-component donor–Por–acceptor systems where they mimic the role of chlorophyll pigment of natural photosynthesis. This is because porphyrins are easy to functionalize, absorb strongly in the visible region, are often highly fluorescent, have rich redox chemistry, and moreover their optical and redox properties are easily tunable.[18] However, most of these model compounds are based on the transition metal porphyrins. Moreover, their photoinduced processes are focused along the plane of the porphyrin. Very few examples are known where the photoinduced processes are in the axial or perpendicular direction to the porphyrin plane.[19–25] This is mainly because of the synthetic challenges where two ligands cannot be attached using transition metal porphyrins.

[a] *Department of Chemistry, University of Prince Edward Island, 550 University Ave., Charlottetown, PE, C1A 4P3 Canada. E-mail: ppoddutoori@upei.ca*
[b] *Department of Chemistry, University of North Texas, 1155 Union Circle, #305070, Denton, TX 76203-5017, USA. E-mail: Francis.DSouza@unt.edu*
[c] *Department of Biological Sciences, Brock University, 500 Glenridge Ave., St. Catharines, ON, L2S 3A1, Canada*

† Electronic supplementary information (ESI) available: Synthesis details, NMR and absorption spectra, titrations (absorption and fluorescence), spectral overlap and transient absorption spectra. See DOI: 10.1039/c5cp04818d

This problem can be addressed by using main group element porphyrins, such as aluminum(III) porphyrin,[26–29] tin(IV) porphyrin[27,30–36] or phosphorus(V) porphyrins,[27,30,37–40] which generally have one or two axial bonds and they can be utilized to attach redox active electron donor (D) and/or acceptor (A) units.

Among the main group porphyrins, aluminum(III)porphyrins (AlPor) are unique, because the axial hydroxide of AlPor reacts with carboxylic acids to form covalent ester linkages while Lewis bases such as pyridine and imidazole form coordination bonds to the Al centre, which is a Lewis acid.[41–46] The combination of these properties makes AlPor a unique candidate for constructing 'axial-bonding' type multi-component D–AlPor–A systems. Over the last few years, we have reported a few novel AlPor based D–AlPor–A systems consisting of three-dimensional (3D) fullerene or two-dimensional (2D) naphthalenediimide as an electron acceptor and ferrocene, tetrathiafulvalene or phenothiazine entities as secondary electron donors.[47–51] In these systems, the EnT and ET reactions were investigated in the axial direction as a function of electronic coupling, orientation, reorganization energy, and the distance between donor and acceptor units. More recently, we reported an AlPor based dyad (AlPor-Ph–H_2Por) where axially bound fluoro-substituted free-base porphyrin (H_2Por) was projected as a two-dimensional (2D) electron acceptor to study the electron transfer in the axial direction.[52] However, due to the strong spectral overlap between AlPor emission and H_2Por absorption, it was found that the H_2Por unit acts as an energy acceptor rather than an electron acceptor. By altering the optical and redox properties of the axial H_2Por unit it is possible to change its role in photoinduced processes. One way to tune the optical and redox properties of the axial H_2Por unit is metalation.

In the present study we have chosen gold(III) as a metal ion because its insertion (that is formation of $AuPor^+$) results in (i) a decrease in spectral overlap between AlPor emission and $AuPor^+$ absorption, (ii) positive shift in redox potentials, and (iii) an increase in the first excited singlet state energy of the acceptor porphyrin ($AuPor^+$). Together with these alterations, electron transfer is expected to outcompete the singlet–singlet energy transfer from AlPor to $AuPor^+$ in the newly synthesized dyad AlPor-Ph–$AuPor^+$ (see Chart 1) and thus guarantee the sequential electron transfer in its corresponding triads (TTF-py→AlPor-Ph–$AuPor^+$ and TTF-Ph-py→AlPor-Ph–$AuPor^+$, see Fig. 1) where the electron transfer could be studied in the axial direction as a function of distance. On the other hand, gold(III) porphyrins are often used as electron acceptors in D–A systems.[53–55] Due to the heavy atom effect of gold metal, its first excited singlet state undergoes rapid intersystem crossing to form a triplet state.[56] The formed triplet state can undergo electron transfer and it can be involved in triplet–triplet energy transfer processes.[57,58] Hence, gold(III) porphyrin as an electron acceptor in the present study will enable us to study the participation of its triplet state in photoinduced processes. We have chosen tetrathiafulvalene (TTF) as the secondary donor because of its strong electron donating ability, which makes it an excellent candidate as a reductive electron quencher or hole acceptor in D–A systems.[24,37,59–61] The general structures of the dyad and its corresponding triads are shown in Chart 1 and Fig. 1, where the TTF and fluoro-substituted gold(III) porphyrin ($AuPor^+$) units are located on opposite faces of the AlPor. We will show that efficient ultrafast electron transfer occurs between AlPor and $AuPor^+$ in the dyad as well as triads. Furthermore, the formed primary charge separated state is stabilized by charge shift from the TTF unit in the case of triads.

2. Experimental section

2.1 Synthesis

All chemicals and solvents used in this study were purchased from either Sigma-Aldrich Chemical Co. or Alfa-Asear. The syntheses of 5,10,15,20-tetra(phenyl)-porphyrinatoaluminum-(III)hydroxide (AlPor-OH) and the reference compound AlPor-Ph have been previously reported.[48] The pyridine appended

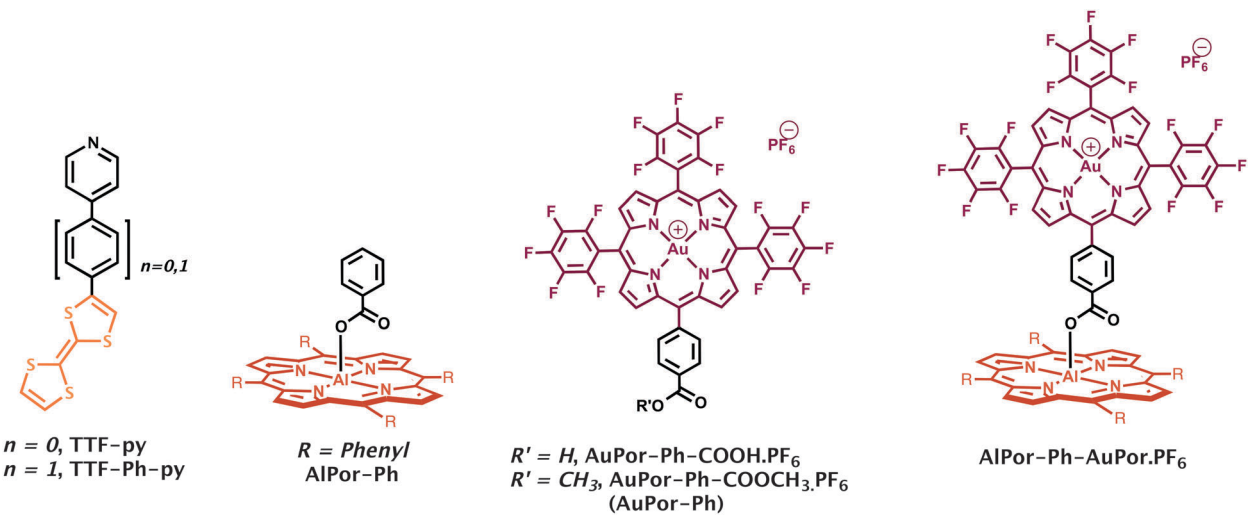

Chart 1 Structural information of investigated compounds in this study.

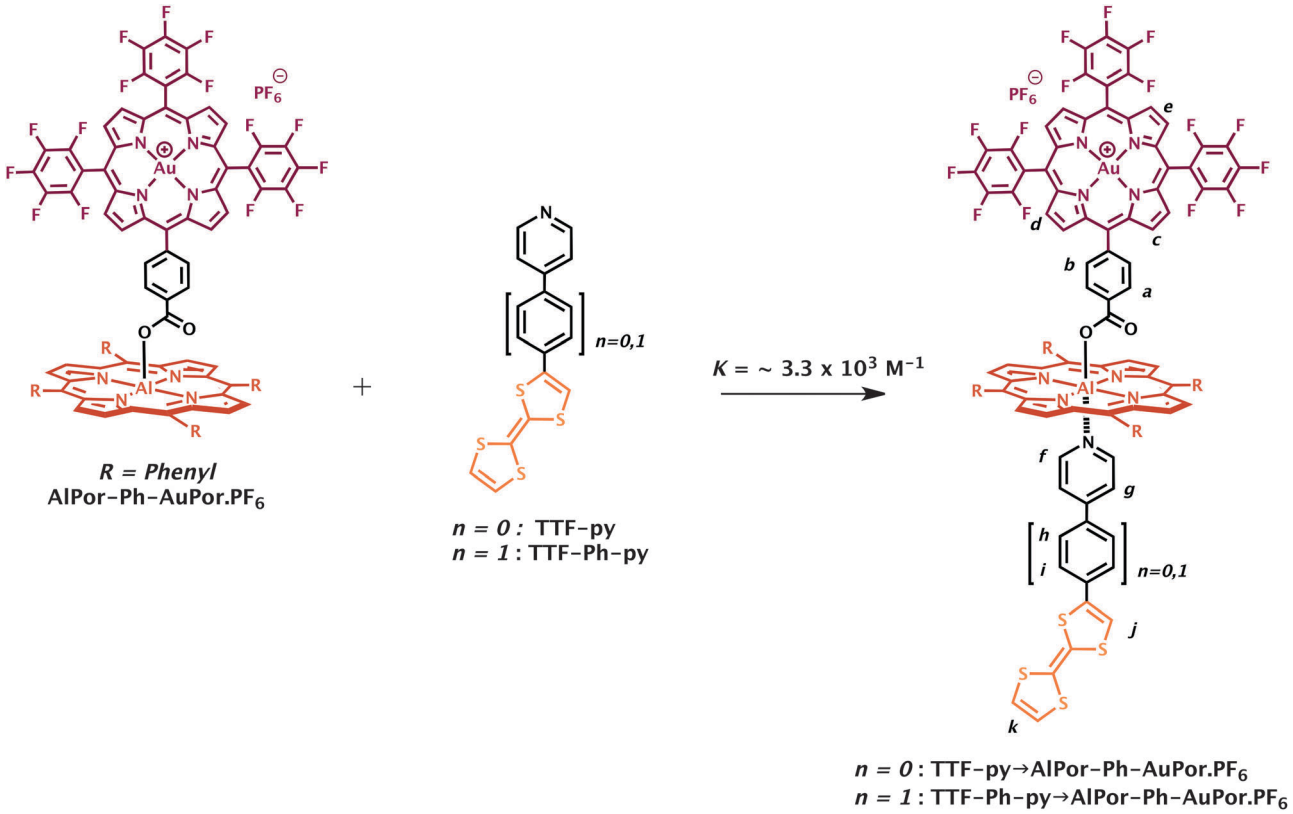

Fig. 1 Formation of vertically arranged self-assembled supramolecular triads through Lewis acid–base interactions.

tetrathiafulvalene derivatives (TTF-py and TTF-Ph-py) and precursor porphyrins (5-(4-methylcarboxyphenyl)-10,15,20-tri(pentafluorophenyl) porphyrin (H_2Por-Ph-$COOCH_3$, from now on referred to as H_2Por-Ph), 5-(4-carboxyphenyl)-10,15,20-tri(pentafluorophenyl)-porphyrin (H_2Por-Ph-COOH)) have been reported elsewhere (Scheme S1, ESI†).[50,52] Gold(III) porphyrin derivatives, 5-(4-methylcarboxyphenyl)-10,15,20-tri(pentafluorophenyl)porphyrinatogold(III) hexafluorophosphate (AuPor-Ph-$COOCH_3$·PF_6, from now on referred to as AuPor-Ph·PF_6) and 5-(4-carboxyphenyl)-10,15,20-tri(pentafluorophenyl)porphyrinatogold(III) hexafluorophosphate (AuPor-Ph-COOH·PF_6), were prepared according to the reported methods[62] (see ESI† for details).

2.2 Preparation of AlPor-Ph–AuPor·PF_6

AlPor-OH (10 mg, 0.015 mmol) and AuPor-Ph-COOH·PF_6 (20 mg, 0.016 mmol) were dissolved in 10 mL of dry dichloromethane. The resulting solution was sonicated for 5 min and then stirred for 12 h at room temperature under a nitrogen atmosphere. The solvent was removed under reduced pressure and washed with hexane to get the pure dyad as a purple solid. Yield: 27 mg (93%). Mass (ESI): *m/z* 1761.2504 $[M–PF_6]^+$, calculated 1761.2516 for $C_{89}H_{40}AlAuF_{15}O_2N_8$. ^{1}H NMR (300 MHz, CD_3CN) ppm: 9.64 (s, 8H), 9.41 (bs, 2H), 9.04 (m, 10H), 8.29 (bs, 8H), 7.79 (m, 12H), 7.34 (bs, 2H), 5.01 (d, 2H, J = 9.0 Hz). ^{1}H NMR ($CDCl_3$, 300 MHz) ppm: 9.42 (bs, 4H), 9.10 (m, 10H), 8.82 (bs, 2H), 8.25 (m, 8H), 7.75 (m, 12H), 7.26 (bs, 2H), 5.60 (bs, 2H). ^{31}P NMR ($CDCl_3$, 121 MHz) ppm: −143.33.

3. Physical methods

3.1 NMR spectroscopy and mass spectrometry

^{1}H NMR, ^{1}H–^{1}H COSY and ^{31}P NMR spectra were recorded on a Bruker Avance 300 MHz NMR spectrometer using $CDCl_3$ or CD_3CN as the solvent. High resolution mass spectrometry analysis was performed on an LTQ Orbitrap Velos mass spectrometer (ThermoScientific) using an ESI ion source operating in positive mode with a resolution of 30 000, monitoring a mass range from 150 to 2000 atomic mass units (amu).

3.2 Voltammetry

Cyclic voltammetric experiments (dichloromethane, 0.1 M tetrabutylammonium perchlorate ($TBAClO_4$)) were performed on the Potentiostat/Galvanostat Model 283 (EG & G Instruments, Princeton Applied Research) electrochemical analyser (working electrode: platinum, auxiliary electrodes: Pt wire; reference electrode: Ag/AgCl). The Fc^+/Fc (Fc = ferrocene, $E_{1/2}(Fc^+/Fc)$ = 0.48 V *vs.* SCE in CH_2Cl_2, 0.1 M $TBAClO_4$ under our experimental conditions) redox couple was used to calibrate the potentials, which were reported in V *vs.* SCE. Spectroelectrochemical studies were performed by using a cell assembly (SEC-C) supplied by ALS Co., Ltd (Tokyo, Japan). This assembly comprised of a Pt counter electrode, a 6 mm Pt gauze working electrode, and an Ag/AgCl reference electrode in a 1.0 mm path length quartz cell. The optical transmission was limited to 6 mm covering the Pt gauze working electrode.

3.3 Steady-state UV-visible absorption and emission spectroscopy

The UV-visible spectra were recorded using a Varian Cary 50 Bio UV-VIS spectrometer. The concentration of the samples used for these measurements ranged from 1×10^{-6} M (porphyrin Soret band) to 5×10^{-5} M (Q-bands) solutions. Steady-state fluorescence spectra were recorded using a Photon Technologies International LS-100 luminescence spectrometer (L-format), equipped with a 70 W xenon lamp, running with Felix software. The low temperature (77 K) spectra were collected using a home built spectrofluorimeter equipped with a Triax 320 spectrograph and a Jobin Yvon Symphony CCD detector. The emission (fluorescence and phosphorescence) data were collected using optically matched solutions; hence the emission intensities are directly comparable.

3.4 Absorption and fluorescence titrations

Absorption titrations were carried out in dry dichloromethane at a concentration of 6×10^{-5} M appropriate for measuring the porphyrin Q bands. A solution containing the acceptor (A = AlPor-Ph–AuPor$^+$ or AlPor-Ph) was placed in a cuvette and titrated by adding aliquots of a concentrated solution of the donor (D = TTF-py, TTF-Ph-py or py). The donor solution also contained the acceptor at its initial concentration so that the porphyrin concentration remained constant throughout the titration. The binding constants were calculated using the Benesi–Hildebrand equation,[63] $[A]/Abs = (1/[D])(1/\varepsilon K) + (1/\varepsilon)$, where [A] is the total concentration of the bound and unbound acceptor and is kept fixed, Abs is the absorption of the complex at the wavelength λ, [D] is the total concentration of the donor which is varied, K is a binding constant and ε is the molar absorptivity of the D–A complex. In an analogous manner, steady-state fluorescence titrations were carried out in dichloromethane using solutions of constant concentration of A and varying concentration of D. The solutions were excited at the isosbestic point wavelength, which was obtained from the corresponding absorption titrations.

3.5 Femtosecond laser flash photolysis

Femtosecond transient absorption spectroscopy experiments were performed using an ultrafast femtosecond laser source (Libra) by Coherent diode-pumped, mode locked Ti:sapphire laser (Vitesse) and a diode-pumped intra cavity doubled Nd:YLF laser (evolution) to generate a compressed laser output of 1.45 W. For optical detection, a Helios transient absorption spectrometer coupled with a femtosecond harmonic generator, both provided by Ultrafast Systems LLC, was used. The source for the pump and probe pulses was derived from the fundamental output of Libra (compressed output 1.45 W, pulse width 100 fs) at a repetition rate of 1 kHz. 95% of the fundamental output of the laser was introduced into the harmonic generator that produces second and third harmonics of 400 and 267 nm besides the fundamental 800 nm for excitation, while the rest of the output was used for generation of white light continuum. In the present study, the second harmonic 400 nm excitation pump was used in all the experiments. The absorbances of AlPor and AuPor are in $\sim$1 : 5 ratio at this excitation wavelength. Kinetic traces at appropriate wavelengths were assembled from the time-resolved spectral data. Data analysis was performed using Surface Xplorer software supplied by Ultrafast Systems. All measurements were conducted in degassed solutions at 298 K.

4. Results and discussion

4.1 Synthesis

Gold(III) metalation was performed by using $AuCl_3$ according to the reported methods.[62] However, low yields (20–25%) were obtained in our experimental conditions. Despite many other decent methods for gold metalation reported in the literature, we used this route due to limitations of our chemical inventory. The counter ion exchange was performed by dissolving the chloride salt in methanol and then precipitating as PF_6 salt by the addition of saturated aqueous NH_4PF_6. The dyad, AlPor-Ph–AuPor$^+$, was prepared in quantitative yields (Scheme S2, ESI†) by reacting equal molar ratios of AlPor-OH and AuPor-Ph-COOH·PF_6 in dichloromethane. Formation of the dyad was monitored by NMR spectroscopy. The obtained dyad was stored in a freshly prepared $CaCl_2$ desiccator prior to optical studies. The triads shown in Fig. 1 were assembled by using the dyad (AlPor-Ph–AuPor$^+$) and TTF-py/TTF-Ph-py derivatives in non-coordinating solvents. Lewis acid–base interactions were utilized to build these vertically arranged supramolecular self-assembled triads. NMR, UV-visible absorption and steady-state fluorescence titrations were employed to monitor the formation of triads. However, the formed self-assembled triads could not be isolated.

4.2 Structural characterization

The mass spectrum of the dyad AlPor-Ph–AuPor·PF_6 showed peaks at 1761 and 639 ascribable to the mass (m/z) of $[M–PF_6]^+$ and $[M–PF_6–\text{axial Por}]^+$, respectively. The ^{1}H NMR spectra of the dyad (AlPor-Ph–AuPor$^+$) and its axial unbound component (AuPor$^+$-Ph-COOH) were measured in $CDCl_3$ and are shown in Fig. S5 (ESI†) (top spectrum) and Fig. S3 (ESI†), respectively. As expected, shielding effects are observed for the proton of axial AuPor$^+$. Protons a and b that appear at 8.55 and 8.25 ppm in the free AuPor$^+$-Ph-COOH compound are shifted to 5.60 and 7.26 ppm, respectively, due to the ring current effect of the porphyrin macrocycle. Similarly, resonances due to the β-protons (c, d and e) are also shifted upfield compared to the corresponding resonances in the spectrum of the compound AuPor$^+$-Ph-COOH. These chemical shifts (δ) agree well with those of axial bonding type porphyrin systems.[47–50,52] However, the observed peaks are very broad and were found to be sensitive towards the concentration of the dyad (see Fig. S5, ESI†). Interestingly, at higher concentration (Fig. S5, ESI,† bottom spectrum) an additional peak at 5.11 ppm was observed for protons a suggesting that in some portion of the sample, the Al centre of AlPor exists in the hexavalent state. In a typical pentavalent AlPor, the Al centre lies out of the porphyrin plane and is pulled into the plane when it converts to the hexavalent complex due to the axial coordination.[47,49,50] If such a phenomenon exists in the dyad solution, the axial AuPor$^+$ could be brought even

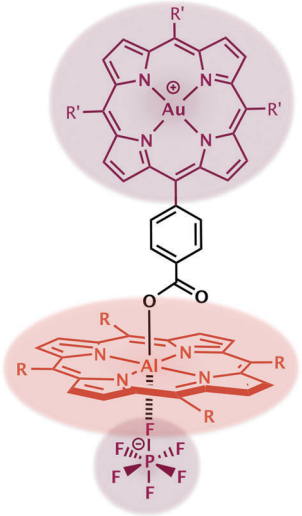

Fig. 2 The proposed hexavalent complex between the PF_6^- ion and the Al center of AlPor in non-coordinating solvents.

closer to the AlPor ring, which may cause an additional shielding on protons a and therefore lower chemical shift. Since the spectrum is measured in a non-coordinating solvent ($CDCl_3$), the possibility of axial coordination by solvent can be safely ruled out. However, careful examination of the dyad structure reveals that the valency conversion is feasible if the counter ion PF_6^- from the dyad molecule is involved in such coordination (Fig. 2). The strong electron withdrawing nature of $AuPor^+$ (which will be discussed in the Electrochemistry section) enhances the Lewis acidity of the Al center that can readily coordinate to a fluorine atom of the PF_6^- ion, which typically acts as a strong Lewis base. Such behaviour has been noticed previously in other systems.[64] This type of Lewis acid–base interaction brings the dyad molecules closer to each other in solution and perhaps forms molecular aggregates. Moreover, this probability would be greater at higher concentrations. Fig. 2 shows the proposed hexavalent complex and it clearly explains the observed broad peaks and additional chemical shift for protons a at higher concentrations in a non-coordinating solvent. In contrast, coordinating solvents (*e.g.* CD_3CN) resulted in a well-resolved spectrum because the solvent is present in large excess and its coordination outcompetes the PF_6^- coordination with the Al centre. Consequently, dyad molecules are expected to lie far from each other in solution. Therefore a well-resolved spectrum is observed (Fig. S6, ESI†). Additionally, the Al centre is continually present in the hexavalent state; hence only one peak is observed for the protons a (at 5.00 ppm). The chemical shift of the ^{31}P NMR signal due to the counter ion in the dyad appears at −143.38 ppm. Overall, the upfield shift of axially linked porphyrin confirms the structure of the investigated dyad molecule.

As shown in Fig. 1, the self-assembled supramolecular triads have been assembled from the components AlPor-Ph–$AuPor^+$ and TTF-py (or TTF-Ph-py). The NMR, UV-visible absorption and fluorescence spectroscopic methods were used to monitor the formation of triads. Fig. S7 (ESI†) shows the ^1H NMR spectrum of a 1 : 1 mixture of AlPor-Ph–$AuPor^+$ and TTF-py. In the coordination complex, shielding due to the porphyrin ring causes an upfield shift of TTF-py protons. The protons f, g, j and k appear at 8.61, 7.26, 6.85 and 6.37 ppm in free TTF-py, whereas in the triad they appear at 6.57, 6.63, 6.57 and 6.29 ppm. The magnitude of the shift depends on the distance of the protons from the porphyrin ring, and the pyridinyl protons (f and g) display the greatest shift indicating that coordination occurs *via* the pyridinyl group. On the benzoate bridging group to the $AuPor^+$, the protons a closest to the porphyrin ring show an increased upfield shift upon coordination. Overall, the observed changes in chemical shift suggest the formation of the self-assembled triad TTF-py→AlPor-Ph–$AuPor^+$. Analogous results were obtained from the triad TTF-Ph-py→AlPor-Ph–$AuPor^+$ (Fig. S8, ESI†).

4.3 UV-visible absorption spectroscopy

The UV-visible spectra of the dyad AlPor-Ph–$AuPor^+$ and the corresponding reference compounds (AlPor-Ph and $AuPor^+$-Ph) were measured in dichloromethane and are shown in Fig. 3a. The band positions (Q-bands and B- or Soret bands) and their molar extinction coefficients are summarized in Table 1. The UV-visible absorption spectrum of the dyad reveals the absorption bands, which correspond to its reference porphyrins AlPor-Ph and $AuPor^+$-Ph. The majority of the absorbance at 406, 415, 520 and 550 nm is attributed to $AuPor^+$ (75%), AlPor (90%), $AuPor^+$ (76%) and AlPor (80%), respectively. The molar extinction coefficients (ε) at 415 and 550 nm, which correspond to the AlPor unit, are slightly lower than those of the reference AlPor-Ph compound. Moreover, the spectrum exhibited a new absorption band at 603 nm and was found to be sensitive to the concentration of the dyad as it appears only at higher concentrations (Fig. 3b). This behaviour is complementary to NMR results and supports the PF_6^- ion binding to the Al centre of AlPor to form the hexavalent AlPor (Fig. 2). The observed new band at 603 nm for AlPor-Ph–$AuPor^+$ is a characteristic feature of hexavalent AlPor.[47,49,50] Additionally, the lower ε values for bands at 415 and 550 nm are also a typical behaviour of hexavalent AlPor as these bands diminish during the conversion of pentavalent to hexavalent Al center.[47,49,50] The py-appended TTF derivatives (TTF-py and TTF-Ph-py) have relatively weak and very broad absorption bands at λ = 304 (average of 285 and 324 nm bands) and λ = 435 nm for TTF-py, and at λ = 298 and 428 nm for TTF-Ph-py (Fig. S9, ESI†).[52] Overall, the absorption studies suggest that there are no interactions between basal (AlPor) and axial porphyrin (H_2Por or $AuPor^+$) units. Furthermore, the absorption bands of AlPor and AuPor are overlapping; therefore by choosing the wavelengths of 550/560 nm and 520 nm it is possible to excite mostly AlPor and the axial $AuPor^+$ units, respectively.

Fig. 4a shows the absorption titrations of TTF-py *vs.* AlPor-Ph–$AuPor^+$ in dichloromethane. Upon addition of the TTF-py, the Q band at 549 nm of AlPor is shifted to 560 nm and also the absorbance at 604 nm increases. The isosbestic point is observed at 555 nm, indicating the formation of the triad TTF-py→AlPor-Ph–$AuPor^+$ in equilibrium, and the changes in the porphyrin bands are typical of axial coordination of nitrogen ligands to AlPor.[47,49,50,52] Benesi–Hildebrand analysis (Fig. 4a, inset) gives a linear plot indicating that a 1 : 1 complex is formed,

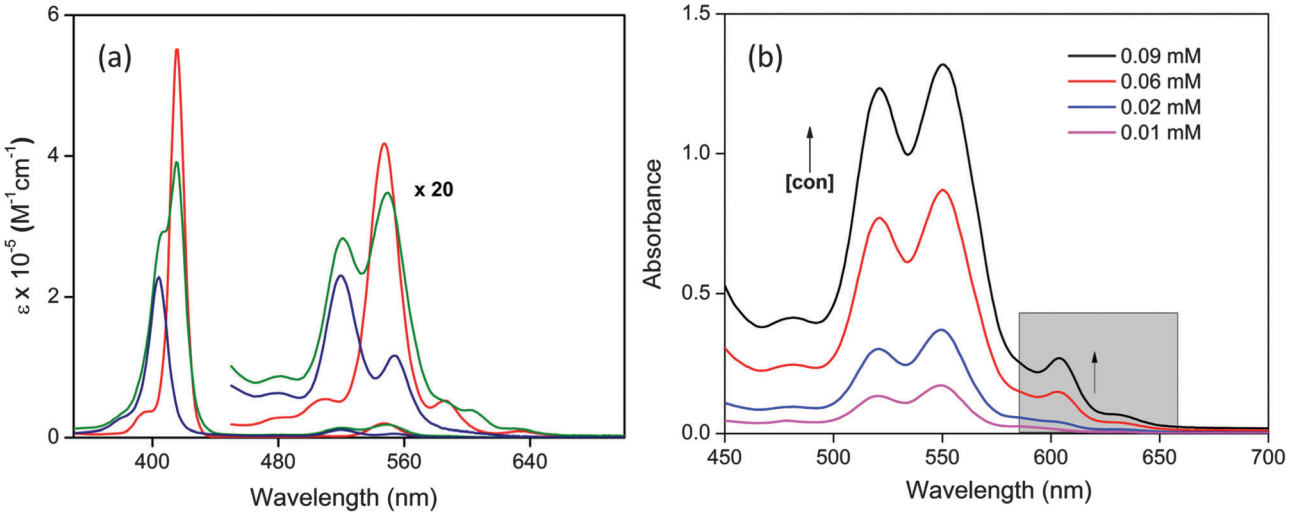

Fig. 3 UV-visible absorption spectra of (a) AlPor-Ph–AuPor$^+$ (green), AuPor$^+$-Ph (blue) and AlPor-Ph (red) in dichloromethane and (b) AlPor-Ph–AuPor.PF$_6$ in dichloromethane at different concentrations.

Table 1 UV-visible absorption, fluorescence and redox potential data of investigated compounds in dichloromethane

	Absorption λ_{max}, nm (log ε)		Fluorescence	Potential (*vs.* SCE)[a]	
Sample	B-bands	Q-bands/TTF	λ_{ex} = 550 nm λ_{em} (%Q)	Oxidation	Reduction
AlPor-Ph	416 (5.74)	585 (3.42), 547 (4.32), 510 (3.44)	595, 646	0.91	−1.21
AuPor$^+$-Ph	404 (5.36)	554 (3.77), 520 (4.06)	—	1.82	−0.28, −0.82
AlPor-Ph–AuPor$^+$	406 (5.46), 415 (5.59)	604 (3.28), 586 (3.41), 549 (4.24), 521 (4.15)	592, 644 (88%)	0.91, 1.16	−0.29, −0.82, −1.20
TTF-py	—	435 (3.45), 324 (4.17), 285 (4.22)	—	0.48, 0.83	—
TTF-Ph-py	—	428 (3.64), 298 (4.48)	—	0.47, 0.87	—

[a] Redox potentials were measured in dichloromethane with 0.1 M TBAClO$_4$ as a supporting electrolyte.

and the slope yields a binding constant (K) ≈ 3.3 × 10^3 M^{-1}. In a similar fashion, the binding constant K was calculated from the titrations of TTF-Ph-py *vs.* AlPor-Ph–AuPor$^+$ (Fig. S10a, ESI†) and was found to be 3.5 × 10^3 M^{-1}. Titrations of TTF-py *vs.* AlPor-Ph and TTF-Ph-py *vs.* AlPor-Ph have been reported elsewhere.[50] Interesting trends were observed in K values. Titrations of TTF-py

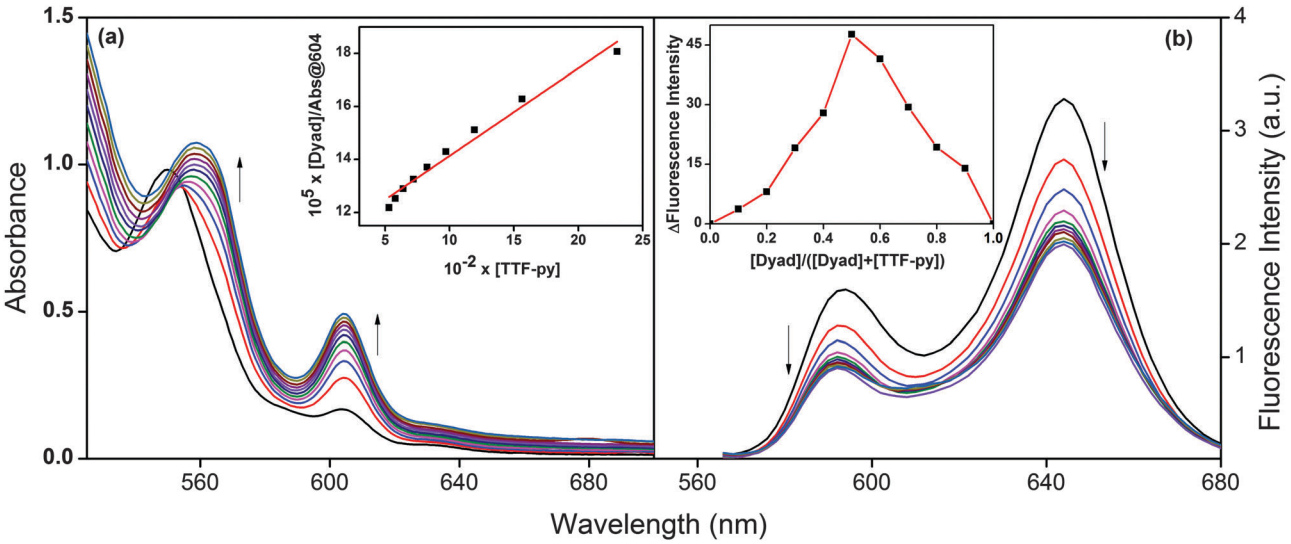

Fig. 4 Titrations of AlPor-Ph–AuPor$^+$ with TTF-py in dichloromethane. TTF-py was added up to 1.88 × 10^{-3} M in 20 μL (2.22 × 10^{-4} M) increments to 1 mL (6 × 10^{-5} M) solution of AlPor-Ph–AuPor$^+$. (a) Absorption titrations: the inset shows the Benesi–Hildebrand plot of the change of absorbance at 603 nm. (b) Fluorescence titrations: the excitation wavelength was chosen at the isosbestic point, 555 nm, obtained from UV-visible titrations. The inset shows Job's plot where the total concentration of [AlPor-Ph–AuPor$^+$] + [TTF-py] was maintained constant at 4.2 × 10^{-5} M.

(or TTF-Ph-py) *vs.* AlPor-Ph–AuPor$^+$ resulted in a higher degree of binding ($\approx 3.3 \times 10^3$ M^{-1}) than that of TTF-py (or TTF-Ph-py) *vs.* AlPor-Ph–H_2Por[52] ($\approx 2.0 \times 10^3$ M^{-1}) and TTF-py (or TTF-Ph-py) *vs.* AlPor-Ph[50] ($\approx 1.0 \times 10^3$ M^{-1}). These results can be explained by the withdrawing nature of the axial subunit as it increases in the order of Ph < H_2Por < AuPor$^+$. The Al center becomes a better Lewis acid and hence it binds strongly with the Lewis base pyridine. Together with NMR and UV-visible absorption titrations, formation of the triads (TTF-py→AlPor-Ph–AuPor$^+$ and TTF-Ph-py→AlPor-Ph–AuPor$^+$) in dichloromethane solutions can be concluded.

4.4 Cyclic voltammetry and energetics

Cyclic voltammetry of the newly investigated dyad and its reference compounds was performed in dichloromethane with 0.1 M TBAClO$_4$. Ferrocene was used as an internal standard. Representative voltammograms are shown in Fig. 5 and the data are summarized in Table 1. The redox processes of all the compounds are found to be one-electron reversible, based on the peak-to-peak separation values and the cathodic-to-anodic peak current ratio. During the cathodic scan, the dyad showed three reduction processes. Based on its monomers, the observed first two processes are assigned to the first and second reduction of the axial AuPor$^+$ unit, whereas the third process is assigned to the first reduction of AlPor. On the other hand, in the anodic scan, the dyad revealed two oxidation processes in our experimental conditions and these are assigned to the AlPor. As anticipated, the dyad exhibited a combination of processes from its monomeric porphyrin units without any perturbation in their redox potentials. Thus, the observed cyclic voltammograms and redox data suggest that the porphyrin units of the dyad do not influence one another significantly. However, the redox potentials of AuPor$^+$-Ph shifted positively compared with its precursor pentafluorophenyl substituted free-base porphyrin (H_2Por-Ph).[52] This is due to the presence of positive charge (+3) on the Au centre, which makes the porphyrin ring further electron deficient. Hence, AuPor$^+$ is reduced at lower potentials and oxidized at higher potentials. The TTF derivatives (TTF-py and TTF-Ph-py) show two processes corresponding to the first and second oxidation of the TTF moiety. These results have been published elsewhere.[50]

Fig. 6 shows the energy level diagram of the dyad and its corresponding supramolecular triads. The redox potentials are used in combination with optical data to estimate the energies of the radical ion pair states (E_{CS}) and free energy change for the charge separation (ΔG_{CS}) by using the Weller equation,[65,66]

$$E_{CS} = e[E_{1/2}(D^{+\bullet}/D) - E_{1/2}(A/A^{-\bullet})] + G_S \quad (1)$$

$$\Delta G_{CS} = E_{CS} - E_{0\text{-}0} \quad (2)$$

where $E_{1/2}(D^{\bullet+}/D)$ is the first oxidation potential of the donor, $E_{1/2}(A/A^{\bullet-})$ is the first reduction potential of the acceptor and G_S is the ion-pair stabilization energy,

$$G_S = \frac{-e^2}{4\pi\varepsilon_0\varepsilon_S R_{D-A}} \quad (3)$$

where R_{D-A} is the centre-to-centre distance between the donor and the acceptor[67] and ε_S is the dielectric constant of the solvent used for the optical and redox studies, in this case dichloromethane. The lowest excited singlet state energy ($E_{0\text{-}0}$) is estimated from the crossing point of absorption and fluorescence spectra and is found to be 579 nm for AlPor.[52] Since AuPor was found to be non-fluorescent, the lower energy band maximum at 554 nm of the absorption spectrum is taken as its

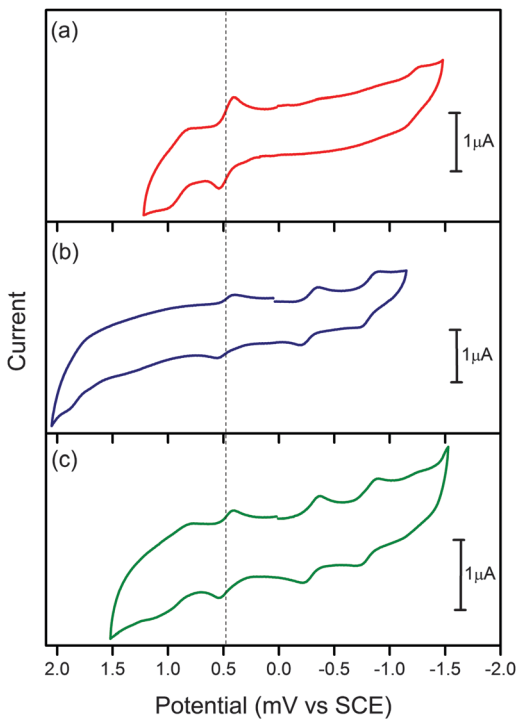

Fig. 5 Cyclic voltammograms of (a) AlPor-Ph, (b) AuPor$^+$-Ph and (c) AlPor-Ph–AuPor$^+$ with 0.1 M TBAClO$_4$ in dichloromethane. Data were measured with ferrocene as an internal standard. Note that the oxidation at 0.48 V in all voltammograms is due to the internal standard ferrocene. Scan rate 25 mV s^{-1}.

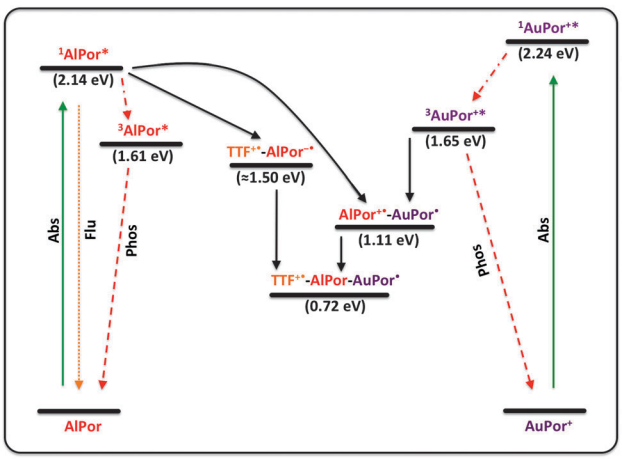

Fig. 6 Energy level diagram of the dyad and its corresponding supramolecular self-assembled triads in dichloromethane. The black solid lines represent electron transfer or hole transfer processes.

lowest excited singlet state. The peak maxima of the phosphorescence band at 769 and 752 nm for AlPor-Ph and $AuPor^+$-Ph respectively (see Fig. 7) are used to estimate the lowest excited triplet states. The calculated free energy levels suggest that the lowest excited singlet state of AlPor (^{1}AlPor*) can be involved in electron transfer and hole transfer with $AuPor^+$ and TTF, respectively, in the triad. However, the sequence of these processes depends on their rates. The calculated energy levels suggest that the triplet–triplet energy transfer from $AuPor^+$ to AlPor and triplet hole transfer from the excited triplet state [^{3}($AuPor^+$)*] to AlPor are also energetically favourable. To verify these schemes, the steady-state fluorescence and the femtosecond transient absorption studies were performed.

4.5 Fluorescence spectroscopy

Fig. 7 illustrates the fluorescence spectra of the dyad and its reference compounds in dichloromethane at room temperature and the data are summarized in Table 1. The $AuPor^+$ was found to be non-fluorescent at room temperature in our experimental conditions. This is due to the heavy atom effect induced by the Au(III) metal ion. As a result, the first excited singlet state of $AuPor^+$ [^{1}($AuPor^+$)*] undergoes rapid intersystem crossing (ISC) to form the triplet state.[56] The dyad fluorescence was measured with an excitation wavelength of 550 nm, where 80% of the light is absorbed by AlPor. As shown in Fig. 7, the dyad revealed two fluorescence bands, which are similar to its reference molecule AlPor-Ph. However, their intensities are strongly (nearly 88%) quenched. Based on the energy level diagram (Fig. 6), where ^{1}($AuPor^+$)* is higher in energy than ^{1}AlPor*, and also due to a weak spectral overlap between AlPor emission and AuPor absorption (Fig. S11, ESI†), the energy transfer from ^{1}AlPor* to $AuPor^+$ can be safely ruled out. On the other hand, the electron transfer from ^{1}AlPor* to $AuPor^+$ is exergonic (ΔG_{CS}) by −1.03 eV. Therefore, the observed strong quenching is attributed to the electron transfer process. However, the heavy atom effect of Au metal cannot be neglected in the excited state properties.

Fig. 4b shows the fluorescence spectra of the AlPor-Ph–$AuPor^+$ dyad with increasing amounts of pyridine-linked tetrathiafulvalene (TTF-py). The excitation wavelength was adjusted to the isosbestic point at 555 nm. In the absence of TTF-py, the dyad showed AlPor bands similar to its monomeric compound AlPor-Ph. However, their intensities were strongly quenched due to the electron transfer from ^{1}AlPor* to axial $AuPor^+$. Upon addition of TTF-py, the fluorescence bands of AlPor were further quenched. These notable spectral changes suggest the formation of the TTF-py→AlPor-Ph–$AuPor^+$ triad in solution. The complexation of AlPor-Ph–$AuPor^+$ with TTF-py in solution was determined by means of Job's plot based on the change in fluorescence intensity. Fig. 4b (inset) shows that a continuous variation plot of fluorescence intensity change *vs.* [AlPor-Ph–$AuPor^+$]/([AlPor-Ph–$AuPor^+$] + [TTF-py]) in dichloromethane gave a maximal value of 0.5, indicating the formation of the TTF-py→AlPor-Ph–$AuPor^+$ complex with a coordination ratio at 1 : 1. To explain the possible quenching mechanism, various control titrations, TTF *vs.* AlPor-Ph–$AuPor^+$ (Fig. S12b, ESI†) and pyridine *vs.* AlPor-Ph–$AuPor^+$ (Fig. S13b, ESI†), were carried out where no change in fluorescence intensity was observed. On the other hand, titrations of TTF-py (or TTF-Ph-py) *vs.* AlPor-Ph revealed a strong quenching in the fluorescence bands of AlPor due to the hole transfer from ^{1}AlPor* to the TTF unit and these results are published elsewhere.[47,50,52] Thus, the most likely explanation for quenching in the triad is an intramolecular photoinduced hole transfer from ^{1}AlPor* to the TTF unit and this process was found to be exergonic (ΔG_{CS}) by −0.64 eV. Similar results were found from the titrations of TTF-Ph-py *vs.* AlPor-Ph–$AuPor^+$ (*i.e.* formation of the triad TTF-Ph-py→AlPor-Ph–$AuPor^+$, Fig. S10b, ESI†). Due to an additional phenyl spacer between the TTF and py units, a decrease in the electronic coupling is expected, which causes a slowdown in the hole

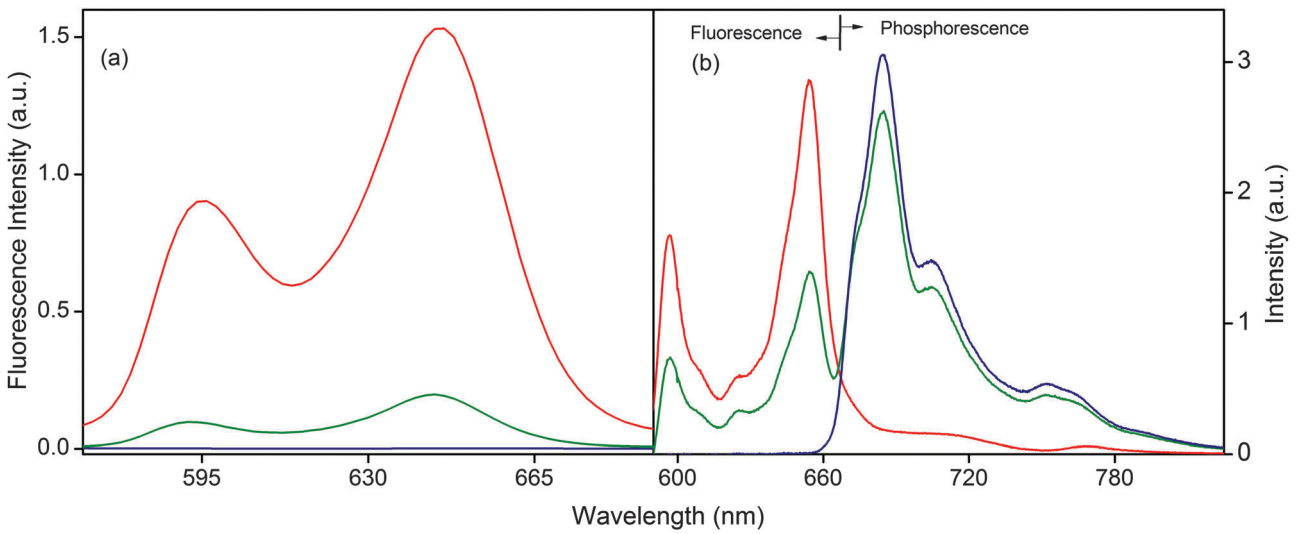

Fig. 7 Emission spectra of AlPor-Ph–$AuPor^+$ (green), AlPor-Ph (red) and $AuPor^+$-Ph (blue) in (a) dichloromethane at room temperature and at an excitation wavelength of 550 nm and (b) dichloromethane : ethanol (=1 : 1) at 77 K and at an excitation wavelength of 520 nm.

transfer rate. Consistent with this expectation, the quenching is weaker. Therefore, the band shifts are more pronounced in the formation of the triad TTF-Ph-py→AlPor-Ph–AuPor$^+$.

To investigate the possibility of hole transfer from ^{3}(AuPor$^+$)* to AlPor in the dyad, the steady-state fluorescence spectra were measured at low temperature. Fig. 7b shows the emission spectra of the dyad AlPor-Ph–AuPor$^+$ and its reference monomers AlPor-Ph and AuPor-Ph in dichloromethane:ethanol (1 : 1) at 77 K. Spectra were measured with excitation at 520 nm where 82% and 18% of the light is absorbed by AuPor$^+$ and AlPor, respectively. The AlPor-Ph showed fluorescence bands at 597 and 654 nm, as well as phosphorescence bands at 710 and 769 nm. In contrast, the AuPor$^+$-Ph displayed only phosphorescence bands at 685, 704 and 752 nm, which were overlapped with the phosphorescence bands of AlPor. As anticipated, the dyad showed a combination of bands, which corresponds to the fluorescence and phosphorescence of AlPor and AuPor$^+$ entities. Furthermore, the fluorescence and phosphorescence bands are quenched by 51% and 14%, respectively. Based on the steady-state fluorescence studies at room temperature, it is reasonable to assign the quenching of AlPor fluorescence bands at 77 K to the electron transfer from ^{1}AlPor* to AuPor$^+$. On the other hand, the singlet–singlet energy transfer from ^{3}(AuPor$^+$)* to AlPor and the hole transfer from ^{1}(AuPor$^+$)* to AlPor are not viable because gold(III) porphyrins are well known to have an extremely short-lived first excited singlet state.[57] In contrast, gold(III) porphyrins typically have a long-lived (usually 1–2 ns, see ref. 53) excited triplet state. Therefore, in combination with suitable energy levels it is likely that the triplet–triplet energy transfer and triplet hole transfer from AuPor$^+$ to AlPor are possible in the investigated dyad at 77 K. However, the results shown in Fig. 7b did not indicate substantial evidence for these processes, *i.e.* the phosphorescence intensity of AuPor$^+$ was not varied significantly in the presence of the AlPor unit. Consequently, we can rule out the possibility of triplet–triplet energy transfer and triplet hole transfer from AuPor$^+$ to AlPor moiety.

4.6 Femtosecond laser flash photolysis

Femtosecond transient absorption studies were performed in *o*-DCB (instead of low boiling dichloromethane) to secure evidence of electron transfer and hole transfer processes in the dyad and triads. Samples were excited using 400 nm wavelength light where the absorbance ratio of AlPor and AuPor$^+$ is approximately 1 : 5. To help interpret the transient spectral data of charge separation products, spectroelectrochemical studies were performed on AuPor$^+$ in *o*-DCB, as shown in Fig. 8. The one-electron reduced product of AuPor$^+$ revealed peaks at 612, 645 (sh) and 790 nm. In addition, the Soret band of AuPor$^+$ located at 409 nm revealed a red-shift of 7 nm and appeared at 416 nm. These processes were found to be fully reversible. Spectroelectrochemical data of AlPor and TTF have been reported previously.[52]

Fig. 9a shows the transient absorption spectrum of AuPor$^+$ at the indicated delay times. In agreement with literature results,[53] the instantly formed S_1 and S_2 states populated long-living triplet excited states *via* the intersystem crossing process.

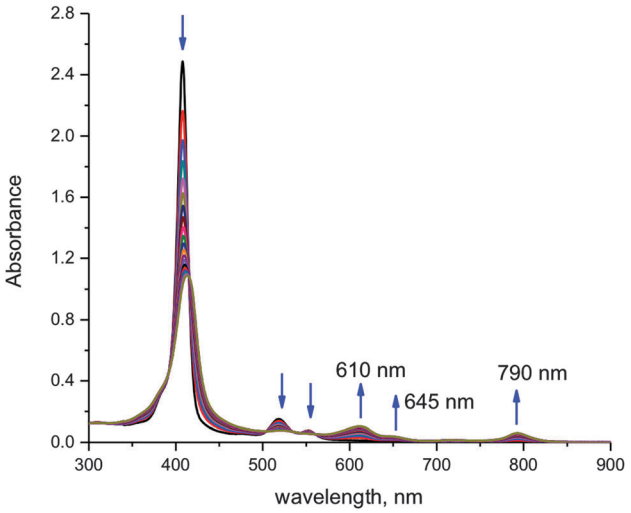

Fig. 8 Spectral changes observed during the first reduction of AuPor$^+$-Ph in *o*-DCB with 0.2 M $TBAClO_4$.

Depleted bands at 520 and 552 nm corresponding to the ground state bleaching of AuPor$^+$ and positive peaks at 585 and 628 nm were observed. Owing to very low fluorescence quantum efficiency, no strong peaks corresponding to stimulated emission of AuPor$^+$ were observed. As expected for the excited triplet state ^{3}(AuPor$^+$)*, the positive peaks decayed slowly as shown by the time profile of the 630 nm peak in Fig. 9b. The decay rate constant was found to be 1.77×10^8 s^{-1} (time constant = 5649 ps) which could be considered as a lower limit since the decay process lasted beyond the monitoring time window of the instrument being 3 ns. The transient absorption spectrum of AlPor is shown in Fig. S14 (ESI†), and it has been reported previously.[52]

Transient spectral features of the AlPor-Ph–AuPor$^+$ dyad are shown in Fig. 10a where in addition to the singlet and triplet features of AlPor and AuPor$^+$, transient spectral features in the 612 nm range and in the 655 nm range (shoulder band to the main ^{3}(AuPor$^+$)* peak) corresponding to the formation of AuPor$^\bullet$ and AlPor$^{+\bullet}$, respectively, are clearly observed. That is, evidence for charge separation in the AlPor-Ph–AuPor$^+$ dyad resulting in the formation of the AlPor$^{+\bullet}$-Ph–AuPor$^\bullet$ radical ion was established. This charge separation could originate from ^{1}AlPor* or ^{3}(AuPor$^+$)*, both having excited state energy sufficient to drive this process (Fig. 6). The earlier discussed phosphorescence studies revealed the absence of significant quenching of ^{3}(AuPor$^+$)* in the dyad at 77 K (see Fig. 7b); however, at elevated temperature electron transfer could occur from this state as the transient peaks of ^{3}(AuPor$^+$)* decay faster in the dyad than in pristine AuPor$^+$. Additionally, no evidence for triplet–triplet energy transfer from ^{3}(AuPor$^+$)* to AlPor was observed indicating that such a process is not competitive. By global fitting of the time profile of the 612 nm peak, time constants for charge separation and charge recombination were obtained. A rise time of 3.16 ps resulted in a rate of charge separation $k_{CS} = 3.17 \times 10^{11}$ s^{-1}, suggesting the occurrence of ultrafast charge separation in the dyad. However, the decay was found to be biexponential (Fig. 10d)

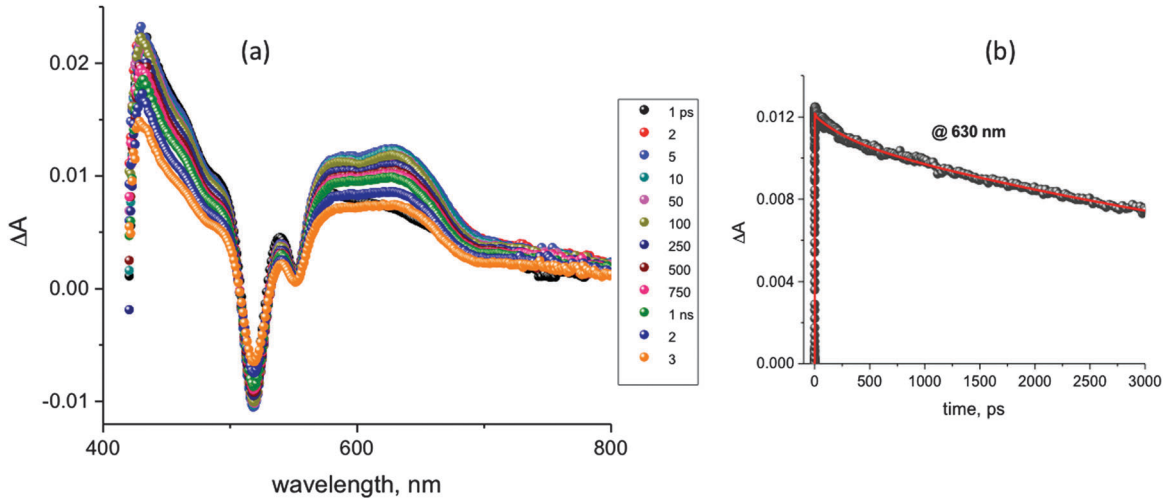

Fig. 9 Femtosecond transient absorption spectra of AuPor$^+$-Ph in *o*-DCB at the excitation wavelength of 400 nm.

with time constants of 27.26 and 2557 ps, resulting in a rate of charge recombination k_{CR} = 3.67 × 10^{10} s^{-1} and 3.91 × 10^8 s^{-1}, respectively. The flexibility of the axially linked AlPor-Ph–AuPor$^+$ dyad has been attributed as the possible cause of the biexponential decay. It is important to mention here that due to the strong overlap of spectral features of AuPor$^\bullet$ and ^{3}(AuPor$^+$)* in the 575–700 nm region, contributions of ^{3}(AuPor$^+$)* in the long-living component cannot be ignored, although the time constant was lower than the time constant of pristine ^{3}(AuPor$^+$)*.

Coordinating TTF-py or TTF-Ph-py to the Al centre of the dyad resulted in TTF-py→AlPor-Ph–AuPor$^+$ and TTF-Ph-py→AlPor-Ph–AuPor$^+$ triads. Fig. 10b and c show the femtosecond transient spectral data of these triads. In both spectra, a peak at 612 nm corresponding to AuPor$^\bullet$ and at 650 nm corresponding to AlPor$^{+\bullet}$ and an additional peak in the 490 nm range corresponding to the formation of TTF$^{+\bullet}$ were observed. These observations are consistent with the formation of TTF$^{+\bullet}$-py→AlPor-Ph–AuPor$^\bullet$ and TTF$^{+\bullet}$-Ph-py→AlPor-Ph–AuPor$^\bullet$ distantly separated radical ion-pairs. By analysing the time profile of the 612 nm peak corresponding to AuPor$^\bullet$ by global fitting (Fig. 10e and f), time constants for charge separation and charge recombination were obtained. In the case of the TTF-py→AlPor-Ph–AuPor$^+$ triad, a rise time of 18.5 ps was obtained resulting in k_{CS} = 5.4 × 10^{10} s^{-1} while the biexponential decay with time constants of 1318 and 1468 ps resulted in k_{CR} values of 7.59 × 10^8 s^{-1} and 6.81 × 10^8 s^{-1}, respectively. For the TTF-Ph-py→AlPor-Ph–AuPor$^+$ triad, the rise and decay time constants of the 612 nm peak were found to be 61.2 and 1484 ps resulting in k_{CS} of 1.64 × 10^{10} s^{-1} and k_{CR} of 6.74 × 10^8 s^{-1}, respectively. For this triad, a monoexponential decay fit was satisfactory to evaluate k_{CR}.

The formation of the final charge separation product in the triads TTF$^{+\bullet}$-py→AlPor-Ph–AuPor$^\bullet$ and TTF$^{+\bullet}$-Ph-py→AlPor-Ph–AuPor$^\bullet$ deserves special mention. There are at least two routes for the formation of these species, *viz.*,

Route 1:

$$TTF–AlPor–AuPor^+ \Rightarrow TTF–AlPor^{+\bullet}–AuPor^\bullet \Rightarrow TTF^{+\bullet}–AlPor–AuPor^\bullet$$

Route 2:

$$TTF–AlPor–AuPor^+ \Rightarrow TTF^{+\bullet}–AlPor^{-\bullet}–AuPor^+ \Rightarrow TTF^{+\bullet}–AlPor–AuPor^\bullet$$

In the first route, the initial photo process involves charge separation in AlPor-Ph–AuPor$^+$ upon photoexcitation (originating from either ^{1}AlPor* or ^{3}(AuPor$^+$)*) to yield the AlPor$^{+\bullet}$–AuPor$^\bullet$ radical ion-pair. In the second step, AlPor$^{+\bullet}$ could undergo subsequent hole shift to TTF to yield the distinctly separated radical ion-pair TTF$^{+\bullet}$–AlPor–AuPor$^\bullet$. In the second route, the initial step involves formation of TTF$^{+\bullet}$–AlPor$^{-\bullet}$ from the ^{1}AlPor* state. In the subsequent step, electron migration from AlPor$^{-\bullet}$ to AuPor$^+$ takes place to yield the TTF$^{+\bullet}$–AlPor–AuPor$^\bullet$ radical ion-pair as the final product. The determined k_{CS} values by monitoring the time profile of AuPor$^\bullet$ for the triads are lower than those observed for the dyad but higher than the hole transfer rates from ^{1}AlPor* to TTF in the TTF-py→AlPor-Ph and TTF-Ph-py→AlPor-Ph control dyads (see Table 2).[52] These results suggest route 1 to be the main electron transfer mechanism. Importantly, k_{CR} values for the distinctly charge separated states of the triads were found to be about two orders of magnitude lower than that observed for the dyad in the absence of coordinated TTF. These results reveal successful charge stabilization in the self-assembled *via* axial position supramolecular triad.

4.7 Role of axial porphyrin (H_2Por *vs.* AuPor$^+$) in dyads and triads

Noticeable differences were observed between the investigated compounds (AlPor-Ph–AuPor$^+$ and TTF-Ph$_n$-py→AlPor-Ph–AuPor$^+$, n = 0, 1) in the present study and the compounds (AlPor-Ph–H_2Por and TTF-Ph$_n$-py→AlPor-Ph–H_2Por, n = 0, 1) that we recently studied.[52] The singlet–singlet energy transfer was found to be the main quenching mechanism in the dyad AlPor-Ph–H_2Por where the axial porphyrin (H_2Por) acted as an energy acceptor. However, the role of H_2Por as an energy

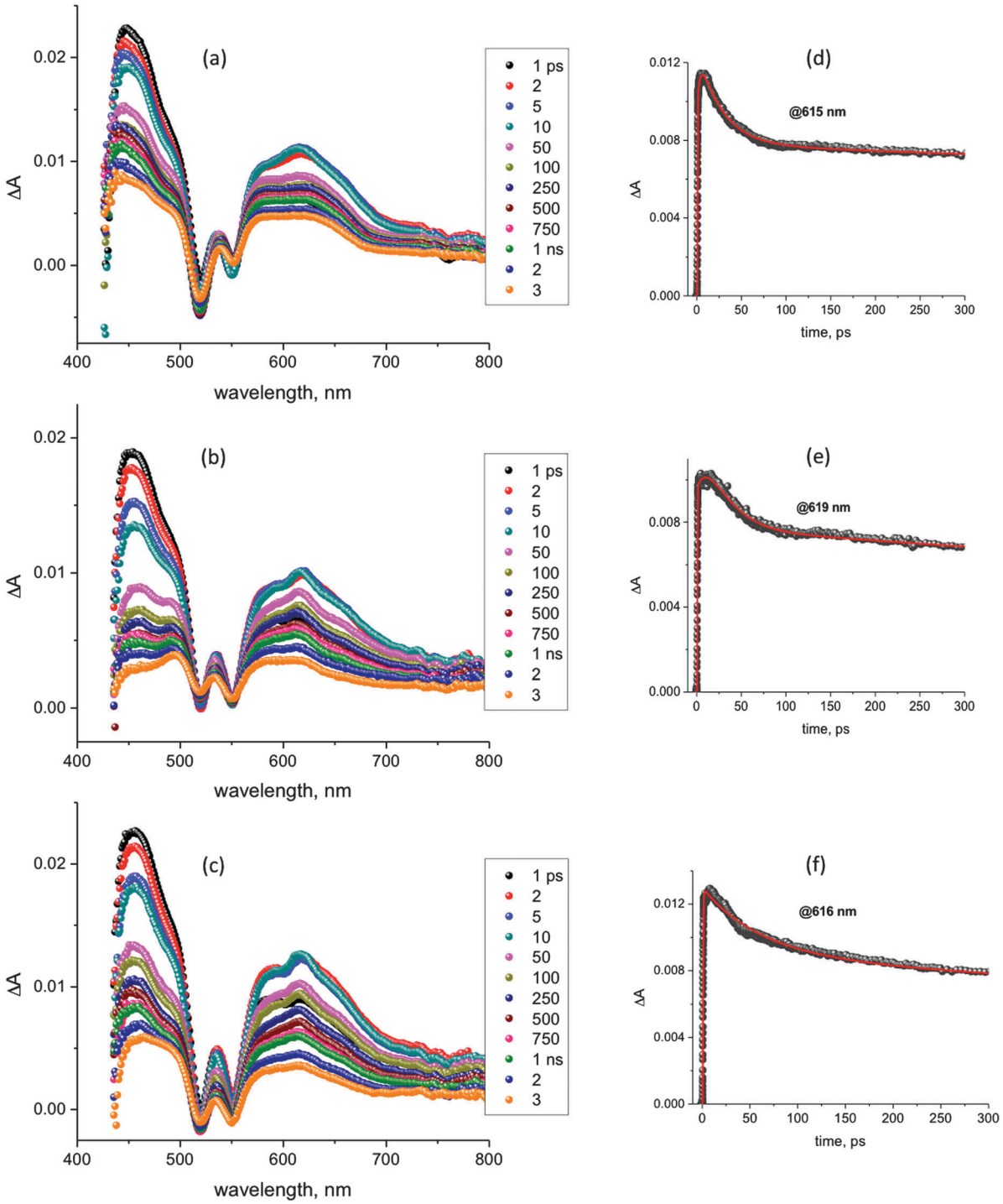

Fig. 10 Femtosecond transient absorption spectra of (a) AlPor-Ph–AuPor$^+$, (b) TTF-py→AlPor-Ph–AuPor$^+$ (3 : 1 ratio), and (c) TTF-Ph-py→AlPor-Ph–AuPor$^+$ (3 : 1 ratio) in *o*-DCB at the excitation wavelength of 400 nm. Figures d, e and f show the time profile of transient peaks of AlPor-Ph–AuPor$^+$, TTF-py→AlPor-Ph–AuPor$^+$ and TTF-Ph-py→AlPor-Ph–AuPor$^+$, respectively.

acceptor was modulated into an electron acceptor by introducing the electron rich TTF molecule to the dyad, that is formation of the triad TTF-Ph$_n$-py→AlPor-Ph–H$_2$Por.[52] In the presence of TTF, the ^{1}AlPor* state is rapidly quenched by the hole transfer to the TTF unit before the transfer of excitation to the H$_2$Por unit. The resulting primary radical pair TTF$^{+\bullet}$-Ph$_n$-py→AlPor$^{-\bullet}$-Ph–H$_2$Por ultimately undergoes a charge shift to H$_2$Por and generates a final radical pair TTF$^{+\bullet}$-Ph$_n$-py→AlPor-Ph–H$_2$Por$^{-\bullet}$. This way, the H$_2$Por entity in the triad was forced to participate as an electron acceptor rather than an energy acceptor.

Interestingly, unlike the case of AlPor-Ph–H$_2$Por, photoexcitation of AlPor in the AlPor-Ph–AuPor$^+$ dyad resulted in an electron transfer

Table 2 Transient data of investigated compounds in *o*-DCB

Sample	τ_{CS} (k_{CS})	τ_{CR} (k_{CR})
AlPor-Ph–AuPor$^+$	3.16 ps (3.12×10^{11} s^{-1})	27.26 ps (3.67×10^{10} s^{-1}), 2557 ps (3.91×10^{8} s^{-1})
TTF-py→AlPor-Ph–AuPor$^+$	18.5 ps (5.40×10^{10} s^{-1})	1318 ps (7.59×10^{8} s^{-1}), 1468 ps (6.81×10^{8} s^{-1})
TTF-Ph-py→AlPor-Ph–AuPor$^+$	61.2 ps (1.64×10^{10} s^{-1})	1484 ps (6.74×10^{8} s^{-1})
TTF-py→AlPor-Ph	80 ps (1.25×10^{10} s^{-1})	—
TTF-Ph-py→AlPor-Ph	120 ps (8.33×10^{9} s^{-1})	—

process from ^{1}AlPor* to the axial porphyrin (AuPor$^+$). The observed differences between the dyads (AlPor-Ph–H_2Por and AlPor-Ph–AuPor$^+$) can be explained by the changes that occur in the optical and redox properties of the axial porphyrin (AuPor$^+$) due to gold(III) metalation. Upon gold(III) metalation, the spectral overlap between AlPor emission and AuPor$^+$ absorption decreases, which prevents the energy transfer process from ^{1}AlPor* to AuPor moiety. Moreover, facile reduction of AuPor$^+$ provides a large driving force for the electron transfer process from ^{1}AlPor* to AuPor$^+$ moiety. Together with these alterations, electron transfer becomes a favourable process between AlPor and AuPor$^+$ in the newly synthesized AlPor-Ph–AuPor$^+$ dyad and its corresponding triads (TTF-py→AlPor-Ph–AuPor$^+$ and TTF-Ph-py→AlPor-Ph–AuPor$^+$). Therefore, upon excitation, the initial charge separation occurs predominantly between the AlPor and AuPor$^+$ units, which results in a primary radical pair (TTF-Ph$_n$-py→AlPor$^{+\bullet}$-Ph–AuPor$^\bullet$). In a consecutive step, the formed radical pair undergoes hole transfer to the TTF unit to produce a spatially well-separated radical pair (TTF$^{+\bullet}$-Ph$_n$-py→AlPor-Ph–AuPor$^\bullet$, designated as route-1) with appreciable lifetimes.

5. Conclusions

The results presented above show the successful mimicking of the vertical type photosynthetic reaction centre TTF–AlPor–AuPor$^+$ by exploiting the unique properties of AlPor, AuPor$^+$ and TTF entities. Ground state properties suggest that there are no intramolecular interactions between molecular components of the triads. However, due to the strong electron withdrawing nature of the axial AuPor$^+$, which induces Lewis acid–base interactions between the Al centre of AlPor and the fluorine atom of counter ion PF_6, intermolecular interactions were found in the dyad. Optical studies revealed that the excitation of AlPor in the triad resulted in ultrafast charge separation predominantly from AlPor to AuPor$^+$ to generate the primary radical pair TTF–AlPor$^{+\bullet}$–AuPor$^\bullet$, which eventually undergoes hole transfer to yield the final radical pair TTF$^{+\bullet}$–AlPor–AuPor$^\bullet$. The resulting TTF$^{+\bullet}$–AlPor–AuPor$^\bullet$ radical pair in the triad has two orders of magnitude slower recombination than the recombination of its parent dyad, *i.e.* AlPor$^{+\bullet}$–AuPor$^\bullet$. Therefore, these results establish the successful charge stabilization in vertical type self-assembled 'D–AlPor–A' supramolecular triads.

Acknowledgements

This work was supported by the Department of Chemistry, University of Prince Edward Island, Canada and the US-National Science Foundation (Grant No. 1401188 to FD). We thank Prof. Russ Kerr and Patricia Boland (Department of Chemistry, UPEI) for mass spectroscopy. R. Kerr acknowledges financial support from the Natural Sciences and Engineering Research Council (NSERC) and the Canada Foundation for Innovation (CFI). Also we thank Prof. Art van der Est and Prof. Melanie Pilkington (Department of Chemistry, Brock University) for providing resources for the synthesis of TTF derivatives.

References

1 J. Barber and B. Andersson, *Nature*, 1994, **370**, 31–34.
2 N. Krauss, W. D. Schubert, O. Klukas, P. Fromme, H. T. Witt and W. Saenger, *Nat. Struct. Biol.*, 1996, **3**, 965–973.
3 M. D. Ward, *Chem. Soc. Rev.*, 1997, **26**, 365–375.
4 M. R. Wasielewski, *Chem. Rev.*, 1992, **92**, 435–461.
5 M. R. Wasielewski, *J. Org. Chem.*, 2006, **71**, 5051–5066.
6 M. R. Wasielewski, *Acc. Chem. Res.*, 2009, **42**, 1910–1921.
7 J. Yang, M. C. Yoon, H. Yoo, P. Kim and D. Kim, *Chem. Soc. Rev.*, 2012, **41**, 4808–4826.
8 N. Aratani, D. Kim and A. Osuka, *Acc. Chem. Res.*, 2009, **42**, 1922–1934.
9 M. S. Choi, T. Yamazaki, I. Yamazaki and T. Aida, *Angew. Chem., Int. Ed.*, 2004, **43**, 150–158.
10 F. D'Souza, S. Gadde, D. M. S. Islam, C. A. Wijesinghe, A. L. Schumacher, M. E. Zandler, Y. Araki and O. Ito, *J. Phys. Chem. A*, 2007, **111**, 8552–8560.
11 S. Fukuzumi, *Phys. Chem. Chem. Phys.*, 2008, **10**, 2283–2297.
12 D. M. Guldi, *Chem. Soc. Rev.*, 2002, **31**, 22–36.
13 D. Gust, T. A. Moore and A. L. Moore, *Acc. Chem. Res.*, 2009, **42**, 1890–1898.
14 H. Imahori, *J. Phys. Chem. B*, 2004, **108**, 6130–6143.
15 Y. Kobuke and K. Ogawa, *Bull. Chem. Soc. Jpn.*, 2003, **76**, 689–708.
16 E. Maligaspe, N. V. Tkachenko, N. K. Subbaiyan, R. Chitta, M. E. Zandler, H. Lemmetyinen and F. D'Souza, *J. Phys. Chem. A*, 2009, **113**, 8478–8489.
17 P. G. Van Patten, A. P. Shreve, J. S. Lindsey and R. J. Donohoe, *J. Phys. Chem. B*, 1998, **102**, 4209–4216.
18 *Handbook of Porphyrin Science*, ed. K. M. Smith, R. Guilard and K. M. Kadish, World Scientific, Singapore, 2010.
19 F. D'Souza, E. Maligaspe, P. A. Karr, A. L. Schumacher, M. El Ojaimi, C. P. Gros, J. M. Barbe, K. Ohkubo and S. Fukuzumi, *Chem. – Eur. J.*, 2008, **14**, 674–681.
20 M. A. Fazio, A. Durandin, N. V. Tkachenko, M. Niemi, H. Lemmetyinen and D. I. Schuster, *Chem. – Eur. J.*, 2009, **15**, 7698–7705.
21 S. Fukuzumi, T. Honda, K. Ohkubo and T. Kojima, *Dalton Trans.*, 2009, 3880–3889, DOI: 10.1039/b901191a.

22 D. I. Schuster, P. Cheng, P. D. Jarowski, D. M. Guldi, C. P. Luo, L. Echegoyen, S. Pyo, A. R. Holzwarth, S. E. Braslavsky, R. M. Williams and G. Klihm, *J. Am. Chem. Soc.*, 2004, **126**, 7257–7270.
23 C. Stangel, C. Schubert, S. Kuhri, G. Rotas, J. T. Margraf, E. Regulska, T. Clark, T. Torres, N. Tagmatarchis, A. G. Coutsolelos and D. M. Guldi, *Nanoscale*, 2015, **7**, 2597–2609.
24 X. W. Xiao, W. Xu, D. Q. Zhang, H. Xu, H. Y. Lu and D. B. Zhu, *J. Mater. Chem.*, 2005, **15**, 2557–2561.
25 Y. Yang, *J. Phys. Chem. A*, 2011, **115**, 9043–9054.
26 P. P. Kumar and B. G. Maiya, *New J. Chem.*, 2003, **27**, 619–625.
27 P. K. Poddutoori, P. Poddutoori, B. G. Maiya, T. K. Prasad, Y. E. Kandrashkin, S. Vasil'ev, D. Bruce and A. van der Est, *Inorg. Chem.*, 2008, **47**, 7512–7522.
28 A. Ghosh, D. K. Maity and M. Ravikanth, *New J. Chem.*, 2012, **36**, 2630–2641.
29 M. Kanematsu, P. Naumov, T. Kojima and S. Fukuzumi, *Chem. – Eur. J.*, 2011, **17**, 12372–12384.
30 L. Giribabu, T. A. Rao and B. G. Maiya, *Inorg. Chem.*, 1999, **38**, 4971–4980.
31 A. A. Kumar, L. Giribabu, D. R. Reddy and B. G. Maiya, *Inorg. Chem.*, 2001, **40**, 6757–6766.
32 H. J. Kim, K. M. Park, T. K. Ahn, S. K. Kim, K. S. Kim, D. H. Kim and H. J. Kim, *Chem. Commun.*, 2004, 2594–2595, DOI: 10.1039/b411482c.
33 T. Lazarides, S. Kuhri, G. Charalambidis, M. K. Panda, D. M. Guldi and A. G. Coutsolelos, *Inorg. Chem.*, 2012, **51**, 4193–4204.
34 V. S. Shetti and M. Ravikanth, *Inorg. Chem.*, 2011, **50**, 1713–1722.
35 L. Giribabu, A. A. Kumar, V. Neeraja and B. G. Maiya, *Angew. Chem., Int. Ed.*, 2001, **40**, 3621–3624.
36 S. V. Bhosale, C. Chong, C. Forsyth, S. J. Langford and C. R. Woodward, *Tetrahedron*, 2008, **64**, 8394–8401.
37 P. K. Poddutoori, A. Dion, S. J. Yang, M. Pilkington, J. D. Wallis and A. van der Est, *J. Porphyrins Phthalocyanines*, 2010, **14**, 178–187.
38 P. K. Poddutoori, J. M. Thomsen, R. L. Milot, S. W. Sheehan, C. F. A. Negre, V. K. R. Garapati, C. A. Schmuttenmaer, V. S. Batista, G. W. Brudvig and A. van der Est, *J. Mater. Chem. A*, 2015, **3**, 3868–3879.
39 K. Hirakawa and H. Segawa, *J. Photochem. Photobiol., A*, 1999, **123**, 67–76.
40 Y. Zhan, K. Y. Cao, C. G. Wang, J. H. Jia, P. C. Xue, X. L. Liu, X. M. Duan and R. Lu, *Org. Biomol. Chem.*, 2012, **10**, 8701–8709.
41 G. J. E. Davidson, L. A. Lane, P. R. Raithby, J. E. Warren, C. V. Robinson and J. K. M. Sanders, *Inorg. Chem.*, 2008, **47**, 8721–8726.
42 G. J. E. Davidson, L. H. Tong, P. R. Raithby and J. K. M. Sanders, *Chem. Commun.*, 2006, 3087–3089.
43 E. Iengo, P. Cavigli, M. Gamberoni and M. T. Indelli, *Eur. J. Inorg. Chem.*, 2014, 337–344.
44 E. Iengo, G. D. Pantos, J. K. M. Sanders, M. Orlandi, C. Chiorboli, S. Fracasso and F. Scandola, *Chem. Sci.*, 2011, **2**, 676–685.
45 G. A. Metselaar, J. K. M. Sanders and J. de Mendoza, *Dalton Trans.*, 2008, 588–590, DOI: 10.1039/b717017n.
46 M. Natali, R. Argazzi, C. Chiorboli, E. Iengo and F. Scandola, *Chem. – Eur. J.*, 2013, **19**, 9261–9271.
47 P. K. Poddutoori, G. N. Lim, A. S. D. Sandanayaka, P. A. Karr, O. Ito, F. D'Souza, M. Pilkington and A. van der Est, *Nanoscale*, 2015, **7**, 12151–12165.
48 P. K. Poddutoori, A. S. D. Sandanayaka, T. Hasobe, O. Ito and A. van der Est, *J. Phys. Chem. B*, 2010, **114**, 14348–14357.
49 P. K. Poddutoori, A. S. D. Sandanayaka, N. Zarrabi, T. Hasobe, O. Ito and A. van der Est, *J. Phys. Chem. A*, 2011, **115**, 709–717.
50 P. K. Poddutoori, N. Zarrabi, A. G. Moiseev, R. Gumbau-Brisa, S. Vassiliev and A. van der Est, *Chem. – Eur. J.*, 2013, **19**, 3148–3161.
51 A. van der Est and P. Poddutoori, *Appl. Magn. Reson.*, 2013, **44**, 301–318.
52 P. K. Poddutoori, L. P. Bregles, G. N. Lim, P. Boland, R. G. Kerr and F. D'Souza, *Inorg. Chem.*, 2015, **54**, 8482–8494.
53 J. Andreasson, G. Kodis, T. Ljungdahl, A. L. Moore, T. A. Moore, D. Gust, J. Martensson and B. Albinsson, *J. Phys. Chem. A*, 2003, **107**, 8825–8833.
54 J. Fortage, J. Boixel, E. Blart, L. Hammarstrom, H. C. Becker and F. Odobel, *Chem. – Eur. J.*, 2008, **14**, 3467–3480.
55 K. Kilsa, J. Kajanus, A. N. Macpherson, J. Martensson and B. Albinsson, *J. Am. Chem. Soc.*, 2001, **123**, 3069–3080.
56 J. Andreasson, G. Kodis, S. Lin, A. L. Moore, T. A. Moore, D. Gust, J. Martensson and B. Albinsson, *Photochem. Photobiol.*, 2002, **76**, 47–50.
57 M. P. Eng, T. Ljungdahl, J. Andreasson, J. Martensson and B. Albinsson, *J. Phys. Chem. A*, 2005, **109**, 1776–1784.
58 L. Flamigni, F. Barigelletti, N. Armaroli, B. Ventura, J. P. Collin, J. P. Sauvage and J. A. G. Williams, *Inorg. Chem.*, 1999, **38**, 661–667.
59 M. Di Valentin, A. Bisol, G. Agostini, P. A. Liddell, G. Kodis, A. L. Moore, T. A. Moore, D. Gust and D. Carbonera, *J. Phys. Chem. B*, 2005, **109**, 14401–14409.
60 G. Kodis, P. A. Liddell, L. de la Garza, A. L. Moore, T. A. Moore and D. Gust, *J. Mater. Chem.*, 2002, **12**, 2100–2108.
61 P. A. Liddell, G. Kodis, L. de la Garza, J. L. Bahr, A. L. Moore, T. A. Moore and D. Gust, *Helv. Chim. Acta*, 2001, **84**, 2765–2783.
62 P. Rothemund and A. R. Menotti, *J. Am. Chem. Soc.*, 1948, **70**, 1808–1812.
63 H. A. Benesi and J. H. Hildebrand, *J. Am. Chem. Soc.*, 1949, **71**, 2703–2707.
64 I. H. A. Badr and M. E. Meyerhoff, *Anal. Chem.*, 2005, **77**, 6719–6728.
65 D. Rehm and A. Weller, *Ber. Bunsen-Ges. Phys. Chem.*, 1969, **73**, 834–839.
66 D. Rehm and A. Weller, *Isr. J. Chem.*, 1970, **8**, 259–271.
67 The structures were optimized by using Avogadro 1.1.1 (W. A. de Jong, A. M. Walker and M. D. Hanwell, *J. Cheminf.*, 2013, 5). The center-to-center distances in AlPor-Ph–AuPor$^+$, TTF-py→AlPor-Ph–AuPor$^+$ and TTF-Ph-py→AlPor-Ph–AuPor$^+$ were estimated to be 12.10 Å, 20.80 Å and 24.85 Å, respectively.

